Crystal structure and magnetic properties of the organic antiferromagnet $(C_1TET\text{-}TTF)_2Br$

Jun-Ichi Yamaura, Akira Miyazaki, and Toshiaki Enoki
Department of Chemistry, Faculty of Science, Tokyo Institute of Technology, O-okayama 2-12-1, Meguro-ku, Tokyo 152, Japan

Gunzi Saito
Department of Chemistry, Graduate School of Science, Kyoto University, Sakyo-ku, Kyoto 606-01, Japan
(Received 26 August 1996)

The organic charge transfer complex $(C_1TET\text{-}TTF)_2Br$ was investigated for its crystal structure, band structure, resistivity, electron spin resonance, and static susceptibility. The crystal structure is characterized by two-dimensional θ-type donor sheets, where the donor arrangement consists of uniform stacking with the absence of dimerized donor molecules. The electrical resistivity shows semiconductive behavior in conflict with the quasi-two-dimensional metallic band structure calculated by the tight binding approximation. These findings show characteristics of the Mott insulating state in this complex. The magnetic susceptibility indicates the feature of an $S=\frac{1}{2}$ two-dimensional triangular lattice Heisenberg antiferromagnet comprising localized magnetic moments on the donor molecules. It shows an antiferromagnetic transition at $T_N=3$ K. [S0163-1829(97)03506-6]

I. INTRODUCTION

In organic charge transfer complexes composed of TTF derivatives, the π-electron systems form a large variety of electronic structures among the superconducting state, charge density wave, spin density wave, and Mott insulating state in low-dimensional frames through the competition among the transfer integral, on-site Coulomb interaction, and electron-phonon interaction.[1–7] In recent years, these complexes have been found to show interesting features in metallic state around the Mott boundary in relation to superconductivity.[8–11] Contrary to this, the complexes belonging to the Mott insulator regime remain not so well understood, although they are expected to give a class of molecule-based low-dimensional magnets. We are interested in the Mott insulating state in the view of the magnetism of the organic charge transfer complexes, because the unpaired electrons delocalized over the molecular π orbitals on the molecules in the Mott insulating state lead to features in their magnetic behavior.[12] Moreover, various types of low-dimensional structures will come to hand on the basis of the modification of the donor molecule arrangements as well as the designing of donor molecules, providing the diversity of magnetic behavior. Consequently, the detailed investigations of organic magnetic insulators will provide aspects of the magnetism in view of the low-dimensional magnetic systems that have been studied in inorganic compounds through many experimental and theoretical approaches.[13,14] In the past, several organic Mott insulators such as α' and β'-$(BEDT\text{-}TTF)_2X$ [$X=AuBr_2$, $CuCl_2$, IBr_2, ICl_2 (Refs. 1–6)] have been targeted as low-dimensional antiferromagnets, in all of which a localized magnetic moment with $S=1/2$ is generated in a BEDT-TTF (abbreviated as ET hereafter) dimer unit associated with dimerized-donor based crystal structures. On the other hand, a class of organic magnetic insulator $(C_1TET\text{-}TTF)_2Br$ (C_1TET-TTF: bis(methylthio)ethylenedithio-tetrathiafulvalene) we synthesized recently, has a uniform donor arrangement with the absence of dimerized structure that most charge transfer complexes of ET have. Thus, the investigations of this compound are expected to reveal interesting features of the magnetic properties among organic magnetic insulators in contrast to ordinary ET salts. Moreover, it is possible to compare the C_1TET-TTF salt with ET salts in detail in view of the crystal structure, electronic structure, and physical properties because the molecular structure of C_1TET-TTF is very close to that of ET. In the present paper, we report the crystal structure, the band structure, the electrical resistivity, electron spin resonance (ESR), and the magnetic susceptibility in order to clarify the correlation between the crystal structure and the magnetic properties.

II. EXPERIMENT

Single crystals of $(C_1TET\text{-}TTF)_2Br$ were prepared by the electrochemical method from C_1TET-TTF and $[(C_2H_5)_4N]_2CuBr_4$ in ethanol under Argon atmosphere at room temperature. In the electrochemical cell, $[(C_2H_5)_4N]_2CuBr_4$ was decomposed into Cu^{2+} and Br^-, so that the produced crystal did not contain even a trace of Cu^{2+} ions, according to energy-dispersive x-ray (EDX) analysis. After the crystal growth period of two weeks, we obtained black plate or block type single crystals with typical dimension of $3\times1\times0.05$ mm^3 or $2\times1\times0.5$ mm^3, respectively. It was found that the crystals with different shapes have the same crystal structure from the x-ray analysis. The found composition is C=28.07, H=2.37, and S=60.25 % from elemental analysis, which is in good agreement with the calculated from the x-ray analysis for $(C_1TET\text{-}TTF)_2Br$ ($C_{20}H_{20}S_{16}Br$); C=28.15, H=2.36 and S=60.12 %.

In the x-ray crystal structure analysis, the intensity data were collected from Rigaku four-circle diffractometer AFC-7S with graphite-monochromated Mo $K\alpha$ radiation using ω-scan technique ($2\theta<55°$), then the absorption was corrected. The structure was solved by the direct method (SHELXS86)[15] and refined using 3536 reflections by full-

TABLE I. Crystallographic data of $(C_1TET\text{-}TTF)_2Br$.

Chemical formula	$C_{20}H_{20}S_{16}Br$
Chemical formula weight	853.23
Cell setting	Monoclinic
Space group	$P2_1/a$
a (Å)	27.71(5)
b (Å)	11.11(2)
c (Å)	5.037(8)
β (°)	90.6(1)
V (Å^3)	1551(4)
Z	2
D_c (Mg m^{-3})	1.827
Radiation type	Mo $K\alpha$
Wavelength (Å)	0.71073
Temperature (K)	293
Crystal size (mm^3)	$0.50\times0.37\times0.33$
No. of independent reflections	3537
No. of observed reflections	$2394(I>2\sigma(I))$
$R[F^2>2\sigma(F^2)]$	0.0685
$wR(F^2)$	0.1988
Weighting scheme	$w=1/[\sigma^2(F_0{}^2)+(0.1452P)^2+1.7684P$, where $P=(F_0{}^2+2F_c{}^2)/3$

matrix least-squares method (SHELXL93).[16] Anisotropic temperature factors were used for all non-hydrogen atoms, and for hydrogen atoms we adopted calculated positions and isotropic temperature factors. The crystallographic data are listed in Table I.

We calculated the molecular orbitals of the $C_1TET\text{-}TTF$ donor on the basis of the extended Hückel method.[17] The transfer integral t was estimated from the overlap integral s using the equation $t=Es$, where the E is the constant value of the order of highest occupied molecular orbital (HOMO) energy -10 eV.[17] The band structure was calculated by means of tight binding method. The HOMO level of the donor is considered to be 3/4-filled from the chemical formula.

The electrical resistivity to the c axis was measured by four-probe method under ambient pressure in the temperature range 190–300 K. ESR measurements were carried out in the applied field parallel to the a^*, b, and c axes in the temperature range 3–300 K, using a conventional X-band ESR spectrometer (JEOL JES-TE200) and a helium continuous flow type cryostat (Oxford ESR910) for temperature control. The magnetic field and the microwave frequency were calibrated by a Gaussmeter (JEOL NMR field meter ES-FC5) and a frequency counter (Advantest microwave counter TR5212), respectively. A single crystal was mounted on a Teflon rod by silicone grease, and sealed in an ESR quartz tube with thermal exchange gas (He 10 Torr). The temperature dependence of the magnetic susceptibility was measured by a superconducting quantum interference device magnetometer (Quantum Design MPMS-5) in the applied field $H=10$ kOe parallel to the a^*, b, and c axes in the temperature range 1.8–400 K. The single crystals, where the crystal axis were collimated, were mounted on a plastic straw with silicone grease. The spin susceptibility was estimated by subtracting the Pascal diamagnetic contribution $\chi_{\rm dia}$ $=-4.49\times10^{-4}$ emu/mol [1 mol=$(C_1TET\text{-}TTF)_2Br$] from the total susceptibility. In the calculation of the core diamagnetic susceptibility, the contribution of $C_1TET\text{-}TTF$ donor is obtained from the observed value $\chi=-2.09\times10^{-4}$ emu/mol of neutral $C_1TET\text{-}TTF$ donor at room temperature.

TABLE II. Fractional atomic coordinates and equivalent isotropic displacement parameters of $(C_1TET\text{-}TTF)_2Br$ (see Fig. 1 for the atom indices). Displacement parameter $U_{\rm eq}$ is defined on the basis of the following equation $U_{\rm eq}=(1/3)\Sigma_i\Sigma_j U_{ij}a_i{}^*a_j{}^*\mathbf{a_i}\mathbf{a_j}$.

Atom	x	y	z	$U_{\rm eq}$/Å^2
C1	0.2260(2)	0.5777(5)	0.1487(11)	0.031(1)
C2	0.1856(2)	0.5759(6)	-0.0123(12)	0.034(1)
C3	0.2918(2)	0.5219(6)	0.4924(12)	0.034(1)
C4	0.3046(2)	0.6300(5)	0.3982(12)	0.034(1)
C5	0.1066(2)	0.5133(6)	-0.2488(12)	0.036(1)
C6	0.1191(2)	0.6174(6)	-0.3662(11)	0.036(1)
C7	0.3748(3)	0.5185(7)	0.8101(13)	0.045(2)
C8	0.3954(2)	0.5902(7)	0.5858(13)	0.044(2)
C9	0.0458(3)	0.3352(9)	-0.0630(17)	0.071(3)
C10	0.0497(3)	0.7886(7)	-0.4296(16)	0.059(2)
S1	0.23882(6)	0.4585(1)	0.3636(3)	0.037
S2	0.26803(6)	0.6927(2)	0.1493(3)	0.041
S3	0.14457(6)	0.4577(2)	-0.0005(3)	0.040
S4	0.17267(6)	0.6860(2)	-0.2488(3)	0.039
S5	0.32184(7)	0.4315(2)	0.7263(4)	0.050
S6	0.35674(6)	0.7127(2)	0.4796(4)	0.047
S7	0.05374(7)	0.4358(2)	-0.3362(4)	0.052
S8	0.08615(6)	0.6865(2)	-0.6222(3)	0.043
Br	0.0000	0.0000	0.0000	0.053

III. RESULTS

At the beginning of this section, we present the crystal structure of $(C_1TET\text{-}TTF)_2Br$. The atomic coordinates and the displacement parameters are listed in Table II and the intramolecular distances and bond angles are in Table III, where the molecular structure and the atom indices are shown in Fig. 1. Also, the crystal structure is shown in Fig. 2. There is one independent donor molecule in a unit cell, while a Br atom is at the position of inversion center. Since all donor molecules are crystallographically equivalent, they are expected to have the same partial charge $+0.5$ taking into account the donor-to-anion ratio of 2:1. There is the absence of disordered sites of ethylene groups and methylthio groups attached to the TTF moieties, although the thermal motions of methylthio groups are a little large. The shortest intermolecular S$\cdots$S contacts are 3.574(6) Å (S3-S8) in the intrastack direction (c axis) and 3.586(7) Å (S6-S7) in the interstack direction (b axis), respectively, which are smaller than the sums of the corresponding van der Waals radii 3.60 Å. As a consequence, $C_1TET\text{-}TTF$ donors form a two-dimensional lattice in the bc plane, where the donor arrangement has zigzag feature with a head-to-tail configuration in the interstack direction. Every $C_1TET\text{-}TTF$ molecule is surrounded by six neighboring donor molecules as shown in Fig. 3, which results in the formation of two-dimensional

TABLE III. Bond lengths and angles of C_1TET-TTF (see Fig. 1 for the atom indices).

Bond length (Å)			
C1-C2	1.377(9)	C5-C6	1.346(9)
C1-S2	1.728(7)	C5-S3	1.740(7)
C1-S1	1.745(6)	C5-S7	1.751(7)
C2-S3	1.737(7)	C6-S8	1.750(7)
C2-S4	1.742(7)	C6-S4	1.765(7)
C3-C4	1.340(9)	C7-C8	1.501(10)
C3-S1	1.748(7)	C7-S5	1.804(8)
C3-S5	1.752(7)	C8-S6	1.810(8)
C4-S2	1.748(7)	C9-S7	1.788(9)
C4-S6	1.758(7)	C10-S8	1.808(8)
Bond angle (°)			
C2-C1-S2	123.8(5)	S3-C5-S7	120.3(4)
C2-C1-S1	120.9(5)	C5-C6-S8	124.4(5)
S2-C1-S1	115.3(4)	C5-C6-S4	116.4(5)
C1-C2-S3	121.3(5)	S8-C6-S4	119.2(4)
C1-C2-S4	123.5(5)	C8-C7-S5	115.1(5)
S3-C2-S4	115.1(4)	C7-C8-S6	113.1(5)
C4-C3-S1	117.0(5)	C1-S1-C3	95.1(3)
C4-C3-S5	128.8(5)	C1-S2-C4	95.3(3)
S1-C3-S5	114.2(4)	C2-S3-C5	95.7(3)
C3-C4-S2	117.2(5)	C2-S4-C6	95.3(3)
C3-C4-S6	127.2(5)	C3-S5-C7	103.3(3)
S2-C4-S6	115.4(4)	C4-S6-C8	99.2(3)
C6-C5-S3	117.6(5)	C5-S7-C9	102.9(4)
C6-C5-S7	122.1(5)	C6-S8-C10	99.8(4)

hexagonal packing structure with the absence of dimerization similar to the θ-ET_2X salt ($X=I_3$, $Cu_2(CN)[N(CN)_2]_2$).[19,20] In view of the symmetry of the structure, the donor molecules of the θ-ET salts are known to locate at centrosymmetric sites, in contrast to the present salt. The dihedral angle is estimated at 57.6(2)° between the molecular planes of adjacent donors interrelated by the screw axis symmetry. We note that the asymmetric donor molecules are oriented in the same direction within a column, which is not so common among the asymmetric TTF derivative salts where donor molecules used to have a head-to-tail configuration in the column except the cases of the present salt and some other C_1TET-TTF salts.[21]

The overlap integrals of the donor HOMO are calculated on the basis of the two-dimensional donor arrangement given

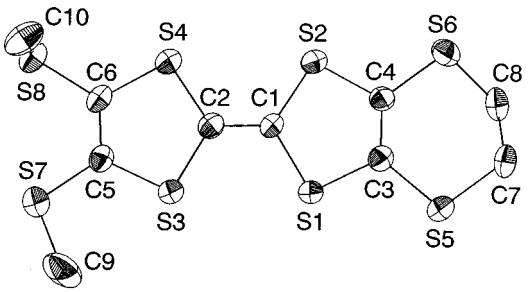

FIG. 1. Molecular structure of C_1TET-TTF drawn by ORTEP (see Ref. 18).

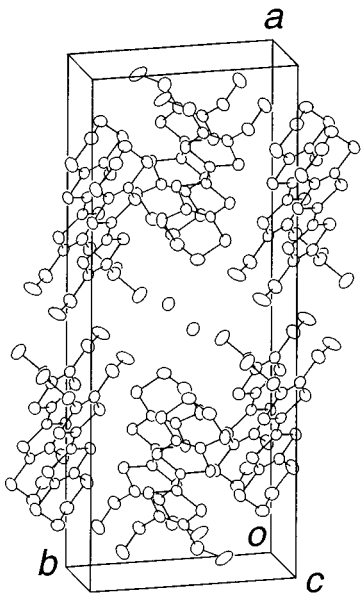

FIG. 2. Crystal structure of $(C_1\text{TET-TTF})_2\text{Br}$.

in Fig. 3, which shows the coexistence of intrastack (c) and interstack (b_1, b_2) interactions. The estimation provides $b_1=5.4$, $b_2=4.3$, and $c=5.8\times10^{-3}$, that reveals a two-dimensional character in the energy band caused by small differences in the strengths of the transfer integrals in all the in-plane directions. Figure 4 shows the band structure and the Fermi surfaces calculated by the tight binding method. The band calculation suggests the presence of two-dimensional metallic bands that generate two sets of quasi-one-dimensional Fermi surfaces, though these band widths are narrow ranging about 0.4 eV due to the small overlap integrals. Since the degeneracy in the M-Y dispersion is caused by the crystallographic symmetry, the 3/4-filled nature is intrinsic. On the other side, the first Brillouin zone has the half-filled feature taking into account the Harrison construction.

The electrical resistivity behaves semiconductive in the investigated temperature range 190–300 K with a single ac-

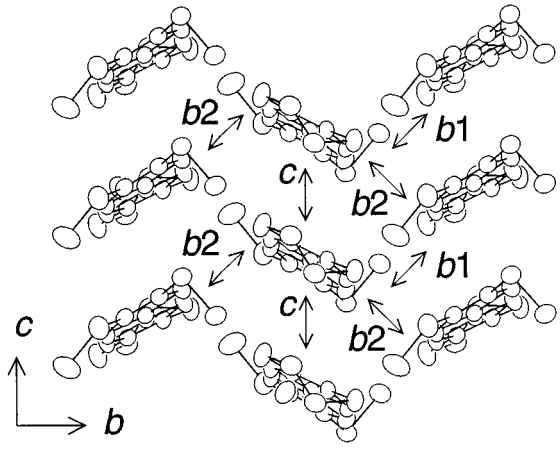

FIG. 3. The arrangement of C_1TET-TTF donors projected on the bc-plane. The calculated overlap integrals are $b1=5.4$, $b2=4.3$, and $c=5.8\times10^{-3}$.

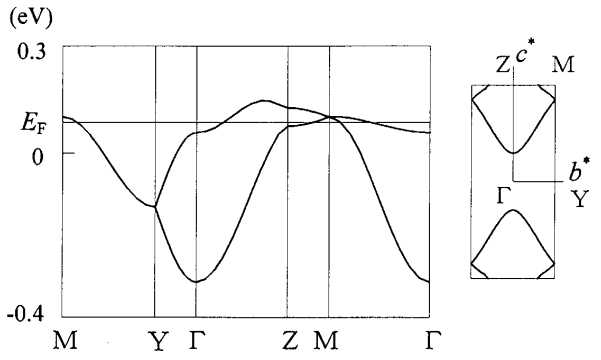

FIG. 4. Band structure and Fermi surfaces of $(C_1TET\text{-}TTF)_2Br$. The energy scale is given on the basis of donor HOMO energy (-10 eV).

tivation energy $E_a=0.6$ eV and the room-temperature resistivity value of $\rho_{rt}=40\ \Omega$cm. This observation is in disagreement with the band calculation which suggests metallic nature. This discrepancy will be discussed later. The ESR signal shows the line shape of single Lorentzian type whose g values and peak-to-peak line widths are $g_{a*}=2.0113$, $g_b=2.0061$, $g_c=2.0055$, and $\Delta H_{a*}=15.6$, $\Delta H_b=14.6$, $\Delta H_c=17.6$ G at room temperature in the applied field parallel to the a^*, b, and c axes, respectively. Taking into account that these g values resemble those of ET donors[22] having similar electronic structure, the unpaired π-electrons observed in the ESR measurements are considered to reside on the C_1TET-TTF molecules. The temperature dependence of the line width and the g value are shown in Fig. 5. The line widths show a weak increase below about 100 K with decreasing the temperature and tend to saturate below about 20

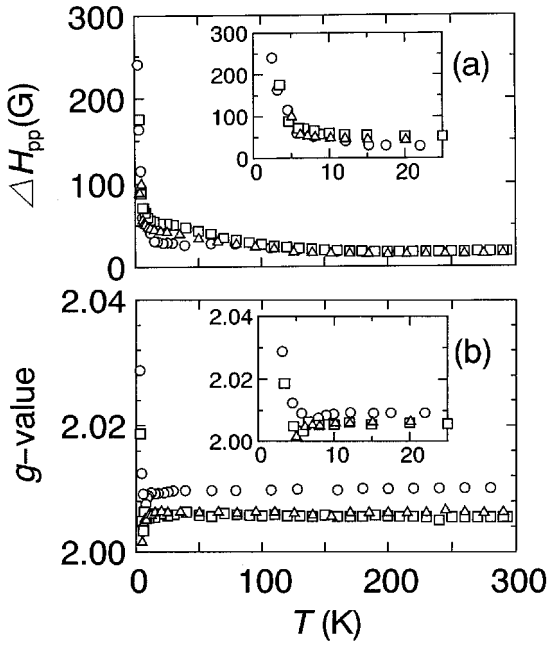

FIG. 5. Temperature dependence of ESR line widths (a) and g values (b) in the applied field parallel to the a^* (○), b (△), and c (□) axes. The insets show the detailed behavior in the low temperature range, which suggest the presence of an antiferromagnetic ordering at $T_N=3$ K.

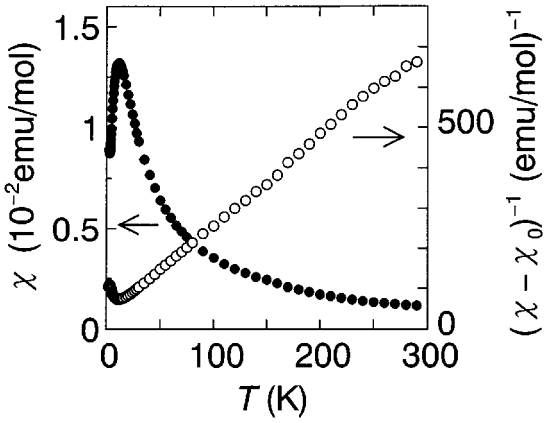

FIG. 6. Temperature dependence of magnetic susceptibility and reciprocal susceptibility in the field of $H=10$ kOe applied parallel to the c axis. $\chi_0=-1.1\times10^{-4}$ emu/mol denotes the temperature-independent term in the susceptibility. The mole unit corresponds to the formula unit of $(C_1TET\text{-}TTF)_2Br$. The best fitting with a single Curie-Weiss contribution gives the spin density $N=1.2$ spin/mol and the Weiss temperature $\theta=-17.3$ K.

K, which suggests the presence of the magnetic short-range order effect. And, they exhibit a broaden out abruptly below 5 K, indicating the onset of antiferromagnetic ordering in the low-dimensional antiferromagnet. The g values show temperature-independent behavior above 20 K and a slight decrease with lowering the temperature below 20 K that is generated by the short-range order effect,[23] and then finally they increase suddenly with the concomitance of the broaden out in the line width below 5 K.

Figure 6 shows the temperature dependence of the magnetic susceptibility and the reciprocal susceptibility as a function of temperature in the applied field parallel to the c axis. The susceptibility shows the Curie-Weiss behavior in the high-temperature range, and then it shows a broad hump of low-dimensional antiferromagnetic short-range order around 12 K, that is considered to be related to the weak increase in the line width observed in the same temperature range. In the temperature range 30–290 K, the susceptibility data in the field parallel to the a^*, b, and c axes are well represented by the sum of a Curie-Weiss term and a temperature independent one after the correction of Pascal diamagnetic contribution;

$$\chi=\frac{C}{T-\theta}+\chi_0. \tag{1}$$

Using this equation, the analysis of the c-axis data gives the Curie constant $C=0.454\pm0.002$ emu K/mol, the antiferromagnetic Weiss temperature $\theta=-17.3\pm0.7$ K and the temperature-independent diamagnetic susceptibility $\chi_0=-1.1\pm0.1\times10^{-4}$ emu/mol, where 1 mol involves one formula unit $(C_1TET\text{-}TTF)_2Br$. These values for the c axis are in good agreement with those for the a^* and b axes. From the Curie constant, the spin density ($S=1/2$) is estimated at $N=1.2$ spin/mol using the ESR g value; namely, there exists one localized magnetic moment of $S=1/2$ in two donors. It is noticeable that the susceptibility contains the temperature independent term χ_0, even after the correction of Pascal diamagnetic contribution χ_{dia}. The magnitude of the χ_0 amount

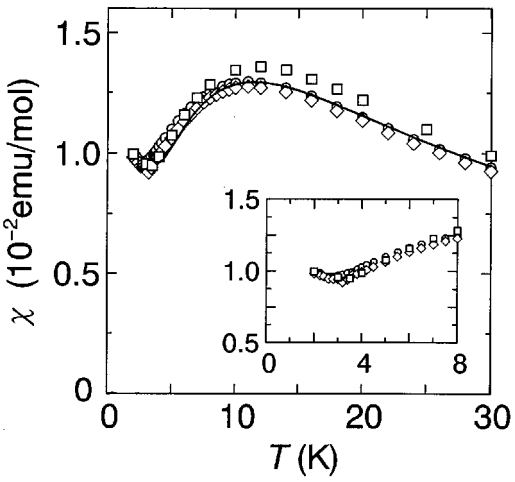

FIG. 7. Temperature dependence of magnetic susceptibility at low temperatures below 30 K in the applied field of $H=10$ kOe parallel to the a^* (□), b (◇), and c (○) axes. The solid line denotes the theoretical fitting for the two-dimensional square lattice Heisenberg antiferromagnet model (Ref. 31) in the temperature range 8–290 K, where 0.5 spin with $S=1/2$ is allotted to one C_1TET-TTF donor according to the charge distribution. The exchange interaction is estimated at $J=-6.1$ K. An antiferromagnetic transition is observed at $T_N=3$ K. The inset shows the detailed behavior in the vicinity of the transition.

about 25% of the $\chi_{\rm dia}$. The origin of the χ_0 is possibly due to be the π-electron ring current in the donor molecule. The correction is expected to be affected by the valence state of the donor, namely, we have used the observed core diamagnetic susceptibility of the neutral donor for the evaluation in the charge transfer complex by neglecting the partial valence feature (+0.5) in the actual case. However, the temperature-independent term is not solely explained by the correction of the core susceptibility because the enhancement in the core diamagnetism of ET complexes having similar extended π-electronic structure to C_1TET-TTF is only 4% from the corresponding neutral donor.[24] Therefore, the origin of the temperature-independent term remains unsolved for $(C_1\text{TET-TTF})_2\text{Br}$.

Figure 7 represents the detailed susceptibility behavior in the temperature region below 30 K in the applied field parallel to the a^*, b, and c-axes. The susceptibilities have an antiferromagnetic short-range order hump around 12 K. The difference of the susceptibility between the a^* axis and the b, c axes is explained by the difference in the g values. Below $T=3$ K, the susceptibility shows an abrupt increase for the a^*, b, and c axes. The behavior of the susceptibility and the ESR line width broadening in the low-temperature range suggest the appearance of an antiferromagnetic order at $T_N=3$ K. It is worth noting the absence of magnetic anisotropy below T_N among the susceptibilities in the field applied parallel to the three independent crystallographic axes. Although a possible explanation for this is the deviation of the easy spin axis from these crystallographic axes, the origin remains unspecified. Magnetization curves in the field parallel to the a^*, b, and c axes at 2 K up to 5 T show a slightly concave with the absence of an apparent spin-flop transition. The concave feature indicates that the large spin reduction in the $S=1/2$ Heisenberg antiferromagnet with quantum spin fluctuation is suppressed by the external field in the ordered state.[25,26]

IV. DISCUSSION

The semiconductive nature with large activation energy and the presence of localized magnetic moments on C_1TET-TTF donors evidence features of Mott insulator generated by the competition between the on-site Coulomb interaction and the transfer integral. Comparison to the reported ET-based Mott insulators[1–6] provides a good suggestion on the electronic structure of the present compound. For instance, α'- and β'-ET_2X-type Mott insulators have intrinsic half-filled bands, which are realized by the band splitting due to the strong dimerization of donor molecules. Thus, in these cases, the competition between the interdimer transfer integral and the effective on-site Coulomb interaction, the latter of which is given by the intradimer transfer integral,[27] generates the Mott insulating state, where the magnetic moment is well localized around the region confined in the dimerized unit of ET molecules. On the contrary, the present compound has the 3/4-filled band structure due to the uniform donor stacking, indicating that this compound is not likely to the ordinary Mott insulator, although the band structure of this compound has the half-filled nature in the first Brillouin zone as shown in Fig. 4. In this sense, the picture of the donor-dimer-based Mott insulating state is failed here, suggesting that the region, where a localized moment exists, is extended widely in a unit cell. Consequently, the features of the electron localization are considered to be situated far from those of Mott insulator state realized in the ordinary ET complexes and are just around the Mott boundary in this compound. Moreover, it is possible that this less localized nature affects the magnetic behavior in $(C_1\text{TET-TTF})_2\text{Br}$.

Now, we discuss the magnetic structure and the exchange interaction mechanism in details. Taking into account that all donors molecules are crystallographically equivalent, all the donor molecules are equally charged due to the charge transfer to anions. Here, it is likely to assume that 0.5 spin with $S=1/2$ exists on a donor molecule within the consideration of the x-ray average structure, although the underlying physics behind it remains to be clarified in the future. The antiferromagnetic exchange interaction $J\propto -t^2/U$ between the donor molecules is described in terms of the transfer integral t and the on-site Coulomb interaction U. Thus, the above consideration leads to the estimation of the exchange interactions $J_1\propto -t_{b1}{}^2/U\sim -t_c{}^2/U$ and $J_2\propto -t_{b2}{}^2/U$ for magnetic neighbors in the different three directions in the bc plane, where the ratio of the exchange interactions is given to be $J_2/J_1\sim 0.5$ from the extended Hückel electronic structure calculation discussed before. From the information on the structure and the band calculation, as shown in Fig. 8, the predominant exchange interactions J_1 form a distorted square magnetic lattice, while J_2 causes the frustration in the spin arrangement. Therefore, the exchange interaction network is described in terms of a triangular lattice with two kinds of antiferromagnetic exchange interactions J_1 and J_2, where the magnetic moments in the distorted square lattice formed by the stronger interactions J_1 are coupled to each

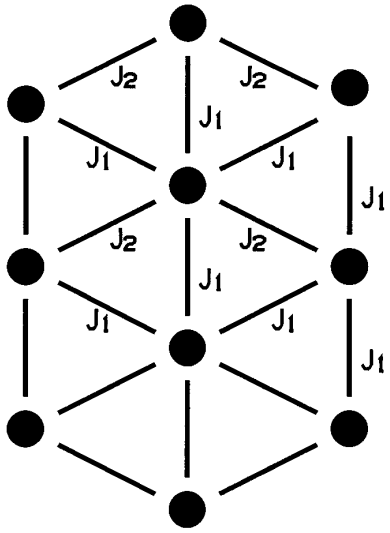

FIG. 8. Schematic representation of the triangular magnetic lattice for the C_1TET-TTF layer with antiferromagnetic interactions J_1 and J_2.

other through the weaker interactions J_2. In the case of $J_1=J_2$, the magnetic system is described as a two-dimensional regular triangular lattice antiferromagnet, which provides interesting models for classical and quantum spins.[28,29] Meanwhile, in the present case having $J_1>J_2$, the magnetic lattice is expected to be the distorted triangular one. It is possible to compare this compound with $CuCl_2$-graphite intercalation compounds (GIC), where Cu^{2+} magnetic moments form an $S=1/2$ two-dimensional distorted triangular lattice Heisenberg antiferromagnet.[30] The susceptibility of $CuCl_2$-GIC has a magnetic short-range order hump characteristic of low-dimensional antiferromagnet around 60 K and no magnetic phase transition above 0.5 K, which is explained by the spin frustration in the $S=1/2$ triangular lattice Heisenberg antiferromagnet.

Here, we examine the presence of the spin frustration in view of the estimation of the exchange interaction in this compound. To our knowledge, there is no theoretical prediction for the susceptibility of the two-dimensional distorted triangular Heisenberg antiferromagnet. Thus, we analyze the susceptibility with a hump by means of the two-dimensional square lattice antiferromagnetic Heisenberg model[31] with predominant exchange constant J_1. The susceptibility is well described by the two-dimensional square lattice Heisenberg antiferromagnet model with the exchange energy of $J_1=-6.1$ K as shown in Fig. 7. It is worth reminding that the estimated exchange interaction is one order of magnitude small in comparison with the exchange interactions of α', β'-ET_2X, and θ-$ET_2Cu_2(CN)[N(CN)_2]_2$ salts. Actually, the transfer integral between the adjacent dimers in α' and β'-ET_2X salts, which have a two-dimensional square antiferromagnetic lattice with dimerized donors having $S=1/2$,[2,4,5] is in the same range to the transfer integrals of the present compound in spite of the large difference in the magnitudes of the exchange interactions. Furthermore, in θ-$ET_2Cu_2(CN)[N(CN)_2]_2$ which has the similar distorted triangular antiferromagnetic lattice[20] to the present compound, the transfer integral is also in the same range. In this case, the ratio of the exchange interactions estimated at $J_2/J_1=0.1$ is considerably smaller than that in the present compound, suggesting that the predominance of J_1 makes spin frustration considerably depressed. Consequently, the difference in the exchange interactions between the present compound and the above ET salts is supposed to be associated with the frustrated spin arrangement through the competition between the antiferromagnetic interactions J_1 and J_2. In other words, the competition between antiferromagnetic J_1 and J_2 is considered to strengthen the features of spin frustration in $(C_1TET\text{-}TTF)_2Br$, resulting in the reduction of the apparent value of the estimated exchange interaction. It is also worth pointing out the importance of the electronic structure for the magnetic features, that is, the less localized nature in the electronic structure, discussed before in relation to the peculiar features realized in Mott boundary, is suggested to cause the reduction in the strengths of exchange interactions in comparison with the ordinary organic magnetic insulators having well localized magnetic moments on the donor molecules.

V. SUMMARY

We investigate the crystal structure and physical properties of the organic antiferromagnet $(C_1TET\text{-}TTF)_2Br$. The donor molecules form two-dimensional θ-type donor arrangements with the absence of donor dimerization that the ordinary ET complexes behaving as Mott insulators have. The resistivity behaves semiconductive with a single activation energy $E_a=0.6$ eV, which is in disagreement with the band calculation. ESR and the magnetic susceptibility prove the presence of localized magnetic moments $S=1/2$ on donor molecules, whose concentration is given to be the assumption of 0.5 spin/donor. These findings appreciablely evidence the features of Mott insulating state in this compound, although the absence of donor dimerization suggests that the magnetic moments are less localized. The temperature dependence of ESR line width broadens out abruptly below 5 K. The susceptibility shows Curie-Weiss behavior having the antiferromagnetic Weiss temperature $\theta=-17.3$ K in the high-temperature range, it shows a broad hump of low-dimensional antiferromagnetic short-range order around 12 K, and finally suggests the presence of antiferromagnetic long-range ordering below $T_N=3$ K. The consideration based on the calculation of the transfer integral reveals the feature of an $S=1/2$ two-dimensional distorted triangular Heisenberg antiferromagnetic lattice with exchange interactions J_1 and J_2 having different strengths ($J_1>J_2$). The fitting to the model of a square lattice Heisenberg antiferromagnet gives the estimate of exchange interaction $J_1\approx-6$ K by neglecting J_2, which is considerably small in comparison with the similar systems belonging to ET complexes. This demonstrates the important role played by the spin frustration in the triangular antiferromagnetic arrangement formed through competition of two antiferromagnetic interactions with different strengths. The less localized electronic state realized in the 3/4-filled band structure is also considered to be responsible for the features of magnetism.

ACKNOWLEDGMENTS

The authors would like to express their sincere thank to Professor Seiji Miyashita at Osaka University, and Professor Hiroyuki Shiba, and Professor Hidetoshi Nishimori at the Tokyo Institute of Technology for fruitful discussion. This work is supported by the Grant-in-Aid for Scientific Research No. 07232216 from the Ministry of Education, Science and Culture, Japan.

[1] M. A. Beno, M. A. Firestone, P. C. W. Leung, L. M. Sowa, H. H. Wang, J. M. Williams, and M.-H. Whangbo, Solid State Commun. **57**, 735 (1993).

[2] S. D. Obertelli, R. H. Friend, D. R. Talham, M. Kurmoo, and P. Day, J. Phys. Condens. Matter **1**, 5671 (1989).

[3] T. Enoki, M. Enomoto, M. Enomoto, K. Yamaguchi, N. Yoneyama, J. Yamaura, A. Miyazaki, and G. Saito, Mol. Cryst. Liq. Cryst. **285**, 19 (1996).

[4] N. Yoneyama, A. Miyazaki, T. Enoki, and G. Saito, in Synth. Met (to be published).

[5] M. Tokumoto, H. Anzai, and T. Ishiguro, Synth. Met. **19**, 215 (1987).

[6] H. Kobayashi, R. Kato, A. Kobayashi, G. Saito, M. Tokumoto, H. Anzai, and T. Ishiguro, Chem. Lett. 89 (1986).

[7] A. Miyazaki, K. Yamaguchi, T. Enoki, and G. Saito, Synth. Met. (to be published).

[8] J. E. Schirber, D. L. Overmyer, K. D. Carlson, J. M. Williams, A. M. Kini, H. Hau Wang, H. A. Charlier, B. J. Love, D. M. Watkins, and G. A. Yaconi, Phys. Rev. B **44**, 4666 (1991).

[9] U. Welp, S. Fleshler, W. K. Kwok, G. W. Crabtree, K. D. Carlson, H. H. Wang, U. Geiser, J. M. Williams, and V. M. Hitsman, Phys. Rev. Lett. **69**, 840 (1992).

[10] Yu. V. Sushko, H. Ito, T. Ishiguro, S. Horiuchi, and G. Saito, Solid State Commun. **87**, 997 (1993).

[11] K. Miyagawa, A. Kawamoto, Y. Nakazawa, and K. Kanoda, Synth. Met. **70**, 969 (1995).

[12] H. M. McConnell, J. Chem. Phys. **39**, 1910 (1963).

[13] L. J. de Jongh and A. R. Miedema, Adv. Phys. **23**, 1 (1974).

[14] *Magnetic Properties of Layered Transition Metal Compounds*, edited by L. J. de Jongh (Kluwer Academic, Boston, 1990).

[15] G. M. Sheldrick, *SHELXS 86, Program for the Solution of Crystal Structures*, University of Göttingen, Germany (1985).

[16] G. M. Sheldrick, *SHELXL 93, Program for the Refinement of Crystal Structures*, University of Göttingen, Germany (1993).

[17] T. Mori, A. Kobayashi, Y. Sasaki, H. Kobayashi, G. Saito, and H. Inokuchi, Bull. Chem. Soc. Jpn. **57**, 627 (1984).

[18] C. K. Johnson, *ORTEP*-II, Report ORNL-5138, Oak Ridge National Laboratory, Tennessee (1976).

[19] H. Kobayashi, R. Keizo, A. Kobayashi, Y. Nishio, K. Kajita, and W. Sasaki, Chem. Lett. 833 (1986).

[20] T. Komatsu, H. Sato, T. Nakamura, N. Matsukawa, H. Yamochi, G. Saito, M. Kusunoki, K. Sakaguchi, and S. Kagoshima, Bull. Chem. Soc. Jpn. **68**, 2223 (1995).

[21] A. Otsuka, H. Yamochi, G. Saito, T. Sugano, M. Kinoshita, S. Sato, K. Honda, K. Ohfuchi, and M. Konno, Synth. Met. **41-43**, 1699 (1991).

[22] T. Sugano, G. Saito, and M. Kinoshita, Phys. Rev. B **34**, 117 (1986).

[23] K. Nagata and Y. Tazuke, J. Phys. Soc. Jpn. **32**, 337 (1972).

[24] M. Kobayashi, T. Enoki, K. Imaeda, H. Inokuchi and G. Saito, Phys. Rev. B **36**, 1457 (1987).

[25] J. C. Bonner and M. E. Fisher, Phys. Rev. **135A**, 640 (1964).

[26] H. Nishimori and S. Miyashita, J. Phys. Soc. Jpn. **55**, 4448 (1986).

[27] The effective on-site Coulomb interaction U_{eff} defined as the on-site Coulomb energy on a dimer unit is given by $U_{\mathrm{eff}}=(U-\sqrt{U^2+4t_{\mathrm{intra}}{}^2})/2+2|t_{\mathrm{intra}}|\sim 2|t_{\mathrm{intra}}|$ $(U\gg|t_{\mathrm{intra}}|)$, where U is the on-site Coulomb energy of the individual donor and t_{intra} is intradimer transfer integral.

[28] H. Kawamura and S. Miyashita, J. Phys. Soc. Jpn. **53**, 9 (1984).

[29] P. W. Anderson, Mat. Res. Bull. **8**, 153 (1973).

[30] M. Suzuki, I. Suzuki, C. Burr, D. G. Wiesler, N. Rosov, and K. Koga, Phys. Rev. B **50**, 9188 (1994).

[31] M. E. Lines, J. Phys. Chem. Solids **31**, 101 (1970).